Development of a Transient Model for Evaluation of Shell and Tube Heat Exchanger with Helical Baffles Applied for SiO_2 Nanofluid

M.L. Magalhães, A.S. Pereira and S.J.M. Cartaxo*

Federal University of Ceará, Department of Chemical Engineering, Brazil

Abstract: While integrated sizing and analysis procedures for helical shell-and-tube heat exchangers are available in the technical literature, the same does not hold for differential transient methods. This work aims to develop a differential transient model for a shell-and-tube heat exchanger with helical baffles with one pass in the shell and two passes in the tubes, considering one-dimensional variation along the length of the equipment. It is intended to determine the fluids temperature profiles and overall heat transfer coefficient along the equipment. Temperature correction factor Ft, heat load and pressure losses were estimated with the model. The thermophysical properties of the fluids were locally evaluated by using published predictive correlations. Simulations were performed using Python framework computing environment assuming a SiO2 nanofluid.

Keywords: Shell-and-tube heat exchanger, helical baffles, nanofluid, modeling and simulation, differential model.

1. INTRODUCTION

Heat exchangers are essential equipment for economically competitive industrial processes, once energy demand is a critical variable. These devices are used to handle and recover heat loads in a chemical process plant. Heat transfer equipment is defined according to its role in the chemical process. Exchangers may recover heat between two process streams, or between a process stream and a utility stream, e.g. cooling water, steam, etc. [1]. These devices exchange energy primarily by convection, as the metal conductive resistance of the pipe is usually negligible compared to the convective resistances.

As many industrial services require high heat loads, it is impossible in such situation to use double pipe hairpins, since they would require an enormous plant area and have several points susceptible to leaks, in this case it is recommended to use shell-and-tube heat exchangers, one of the most versatile heat exchangers types. Its versatility is a consequence of having a large heat transfer area and demanding a small plant space compared to other types of equipment. Shell-and-tubes heat exchangers with fractional baffles may be evaluated using the method proposed by Kern [1].

When the pressure loss is a critical variable, the use of shell-and-tube heat exchangers with helical baffles is recommended because of its low pressure drop/overall coefficient ratio. These devices possess inclined baffles that force the shell fluid to flow helically, resulting in lower pressure drop than that caused by the crossed flow in a standard shell-and-tube heat exchanger.

*Address correspondence to this author at the Federal University of Ceará, Department of Chemical Engineering, Brazil; E-mail: samuel@ufc.br

2. METHODOLOGY

In this work, calculation procedures of the heat transfer coefficients and pressure drop in the shell and pipes were presented according to the method proposed by Tao *et al*. [2]. The thermophysical properties were locally calculated by using prediction equations for water and SiO_2 nanofluids. The physical properties were considered constant in the fluid energy balance since they were calculated separately based solely on the local temperature. The models developed in this work were implemented in the Python framework, using the scientific modules math, scipy, numpy and matplotlib.

2.1. Shell and Tube Heat Exchangers with Helical Baffles

Figure **1** illustrates the arrangement of baffles for this type of equipment, where the particular features of such kind of baffles are depicted. Typically, a perforated disk is cut in four parts, each one comprising a single baffle. The baffles are fixed with the help of tirods along the tube bundle, forming a pattern which

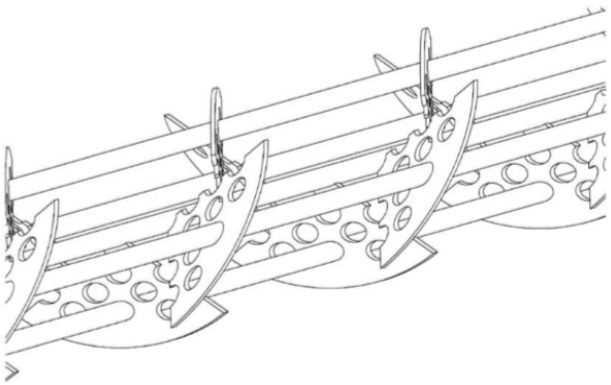

Figure 1: Helical baffle arrangement. Source: Tao *et al*. [2].

E-ISSN: 2409-5826/18

forces the shell-side fluid flow to follow a helical pattern.

The integral analytical method developed by Tao *et al*. [2] is usually recommended to evaluate this equipment. The first step is to obtain the shell-side and tube-side heat transfer coefficients. The film coefficient of the shell was calculated by the correlations found in Schlunder [3] and Stehlik *et al*. [4]. These correlations use Y correction factors to adjust the film coefficient in order to take account of the different flow pattern in helical baffled exchangers compared to the standard baffled one. The film coefficient of the tubes was obtained from the equation proposed by Sieder and Tate [5] for turbulent flow, and from the correlations developed by Gnielinski [6] or Sieder and Tate [5] for laminar flow.

The second step consists in analyzing the pressure drop in the equipment. The shell pressure drop was estimated through the equations developed by Stehlik *et al*. [4]. These equations contain correction factors that are similar to the Y factors found in the film coefficient equations, they are called Z factors and their role is to correct flow conditions. The pressure loss in the tubes was calculated by the equations proposed by Gaddis and Gnielinski [7], Kuppan [8] and Xiao *et al*. [9].

2.2. Physical Properties for Nanofluid

From the experimental data found in Perry [10] and Poling [11], regressions were performed to propose correlations and predict water physical properties. Equations (1), (2), (3) and (4) represent the specific heat, thermal conductivity, density and dynamic viscosity, respectively.

$$c = 9.998 \cdot 10^2 \left(-10^{-7} \left(\frac{T-32}{1.8} \right)^3 + 4.10^{-5} \left(\frac{T-32}{1.8} \right)^2 + 4.212 \right) \quad (1)$$

$$k = 1.7307347(0.31512 + 4.71277 \cdot 10^{-4} T) \quad (2)$$

$$\rho = 0.0000201\, T^3 - 0.022861\, T^2 + 8.0115\, T + 107.071 \quad (3)$$

$$\mu = 0.004134(0.23496 + 3.0222 \exp(-T / 54.20905)) \quad (4)$$

The nanofluids physical properties were evaluated at different temperatures and concentrations. Equation (5) represents the nanofluid density, considering the weighted average of water and suspended particles. The specific heat correlation is given by Equation (6) [12].

$$\rho_{nf}(1-\phi)\rho_f + \phi\rho_p \quad (5)$$

$$c_{nf} = \frac{\phi\rho_p c_p + (1-\phi)\rho_f c_f}{\rho_{nf}} \quad (6)$$

Equations (7) and (8) represent the thermal conductivity and dynamic viscosity, respectively [13]. These correlations are limited to metals and water dispersed metal oxides in low concentrations (below 4%) with particle diameters smaller than 170 nm and temperatures below 70º C.

$$k_{nf} = 0.8938 k_f \left(1 + \frac{\phi}{100} \right)^{1.37} \left(1 + \frac{T_{nf}}{70} \right)^{-0.2777} \left(1 + \frac{d_p}{170} \right)^{-0.0336} \left(\frac{\alpha_p}{\alpha_f} \right)^{-0.0336} \quad (7)$$

$$\mu_{nf} = \mu_f \left(1 + \frac{\phi}{100} \right)^{11.3} \left(1 + \frac{T_{nf}}{70} \right)^{-0.038} \left(1 + \frac{d_p}{170} \right)^{-0.061} \quad (8)$$

Physical properties of the SiO_2 particles [14] are show in Table **1**.

Table 1: Physical Properties of Metal Oxide Nanomaterials

Specific Heat	Density	Thermal Conductivity
745 J/Kg.K	2220 Kg/m3	1.4 W/m.K

2.3. Friction Factor for the Nanofluid

The friction factor, which is function of the Reynolds number, was determined by fitting the data found in Kern [1]. Equations (9) and (10) were used to estimate the friction factor for the shell-and-tubes, respectively.

$$f_{shell} = \left(\left(1.56487\, Re_{shell}^{-0.17512} \right)^{1/0.23718} + \left(51.36493\, Re_{shell}^{-0.94374} \right)^{1/0.23718} \right)^{0.23718} \quad (9)$$

$$f_{tube} = \left(\left(63.85951\, Re_{tube}^{-0.97662} \right)^{1/0.06649} + \left(0.45017\, Re_{tube}^{-0.26729} \right)^{1/0.06649} \right)^{0.06649} \quad (10)$$

Equation (11) was included to calculate the friction correction factor for SiO2 / water nanofluid with the following restrictions: 6800 < Re < 30000, 5.00 ≤ Pr ≤ 7.24, φ ≤ 3% [15].

$$\frac{f_{nf}}{f} = 1.4 \left(0.001 + \frac{\phi}{100} \right)^{0.05} \quad (11)$$

3. MATHEMATICAL MODEL

The simplifying assumptions of the model developed in this work are:

- One-dimensional temperature variation.
- Multi-tubular heat exchanger with one shell-side and two tube-side flow passages.
- Energy balances carried to allocate the hot fluid in the shell-side and the cold fluid in the tube-side.
- Fluids in liquid state, with no phase transition.
- Tubes equally divided between the two passes.
- Inlets nozzles on opposite sides.
- Metal conductive resistance negligible.
- Shell-exterior terminally isolated.
- Newtonian Fluids.

3.1. Energy Balance for the First Pass in the Tubes

Figure **2** illustrates a representative control volume for the energy balance in the tubes. Assuming that $\Delta x \to 0$, a Taylor series truncated at the first-order term gives:

$$wct_1 - \left(wct_1 + \frac{\partial(wct_1)}{\partial x}dx\right) + 0.5\ N_t\ U_1 P\ dx(T - t_1) = \frac{\partial(0.5\ \rho_t\ S_t\ c\ t_1\ dx)}{\partial t} \quad (12)$$

By applying the aforementioned simplifying assumptions, the energy balance was found to be:

$$\frac{\partial t_1}{\partial t} = \frac{1}{0.5\ \rho_t\ S_t\ c}\left(-wc\frac{\partial t_1}{\partial x} + 0.5\ N_t\ U_1 P(T - t_1)\right) \quad (13)$$

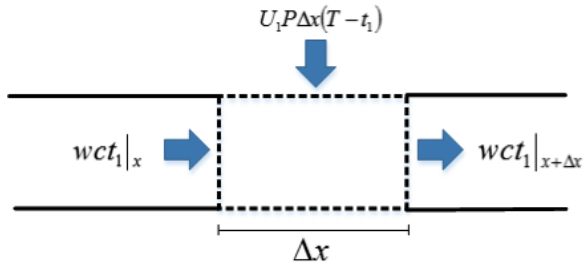

Figure 2: Control volume of tube on the first tube pass.

3.2. Energy Balance for the Second Pass in the Tubes

The energy balance for the second pass of the tubes is similar to the equation developed in the previous section. However, there is a difference in the flow direction, which is the opposite of the considered axes convention. Thus, the energy balance for the second pass resulted in Equation (14):

$$\frac{\partial t_2}{\partial t} = \frac{1}{0.5\ \rho_t\ S_t\ c}\left(wc\frac{\partial t_2}{\partial x} + 0.5\ N_t\ U_2 P(T - t_2)\right) \quad (14)$$

3.3. Energy Balance for Pass in the Shell

In practice, a heat exchanger with more than ten baffles approximates reasonably a uniform temperature on the axial cross section. Accordingly, the reference area of the shell fluid flow (S_c) is defined as the difference between the shell and the tubes cross-sectional areas, as illustrated with the hatched area of Figure **3**. The shell-side equation describing the temperature variation of the shell-side stream is:

$$\frac{\partial T}{\partial t} = \frac{1}{\rho_c\ S_c\ C}\left(WC\frac{\partial T}{\partial x} - 0.5 N_t P(U_1(T - t_1) + (U_2(T - t_2))\right) \quad (15)$$

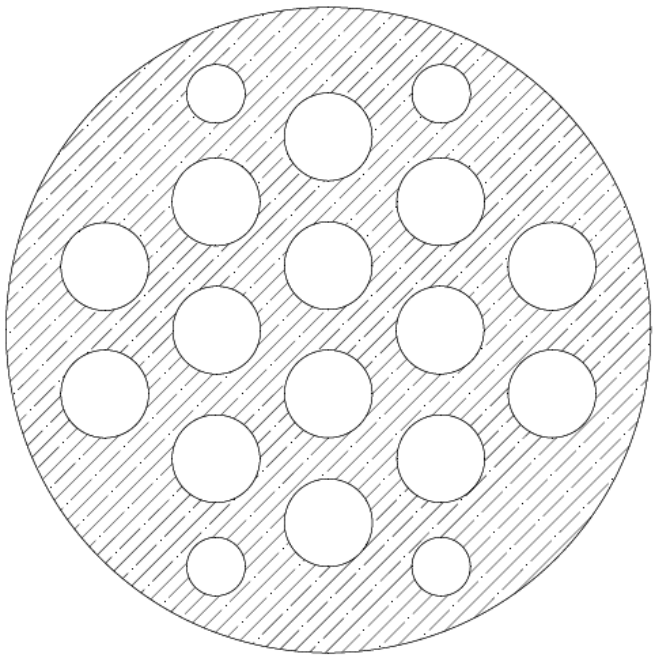

Figure 3: Reference cross section of the exchanger.

4. RESULTS AND DISCUSSION

4.1. Temperature Distributions

The system composed by Equations (13), (14) and (15) was solved numerically considering the variation of the nanofluid properties with the temperature along the heat exchanger. The influence of the concentration of SiO_2 particles on the transport physical properties are shown in Figure **4**.

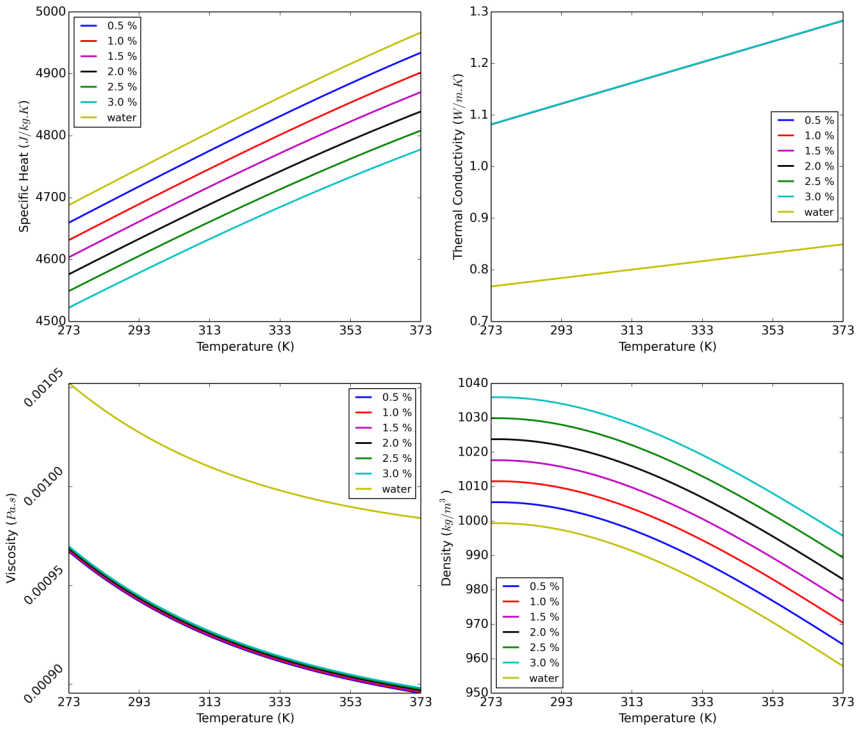

Figure 4: Physical properties for various concentrations of SiO_2 / water nanofluid.

Figure **5** to **12** show the typical behavior of the temperature distribution for the hot and cold fluids along the length during the transient period.

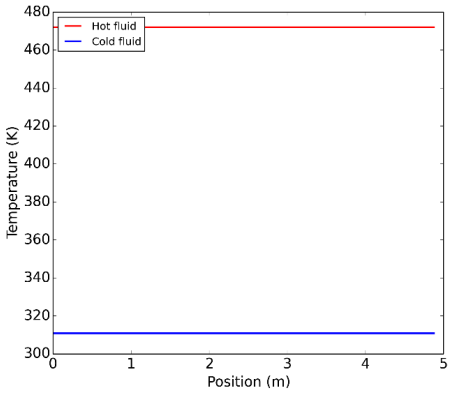

Figure 5: Temperature distribution in 0 s.

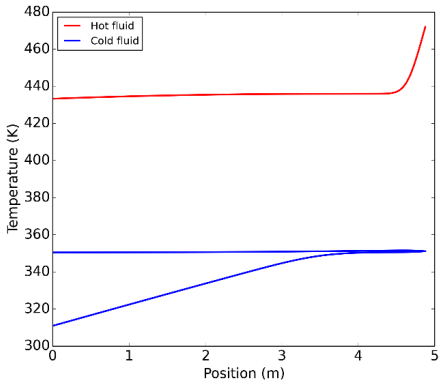

Figure 6: Temperature distribution in 3 s.

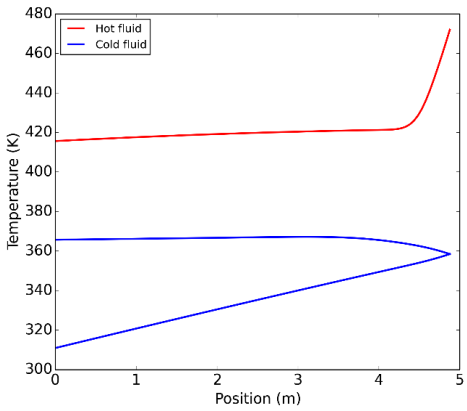

Figure 7: Temperature distribution in 5 s.

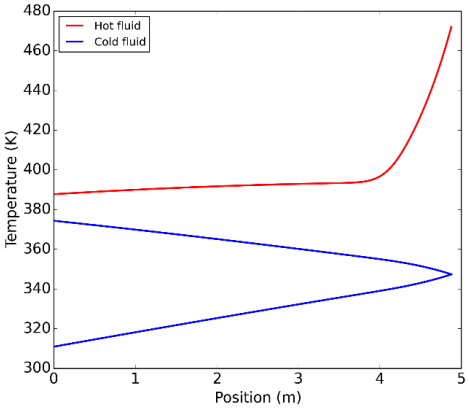

Figure 8: Temperature distribution in 10 s.

Table 2: Exchanger Specifications

Shell	DI 0.387 m	LTC 4.877 m	LTO 4.572 m	Bd 0.305 m	Sp 10.0 mm	Db 0.077 m	β 44.0°
Tube	N_t 160	de 0.019 m	di 0.016 m	df 0.387 m	pt 23.812 mm		

Table 3: Operating Conditions

Shell	T_1_e 306.89 K	w 22.049 kg/s	Pitch Triangular	Water
Tube	t_1_e 296.89 K	w 35.279 kg/s		Water

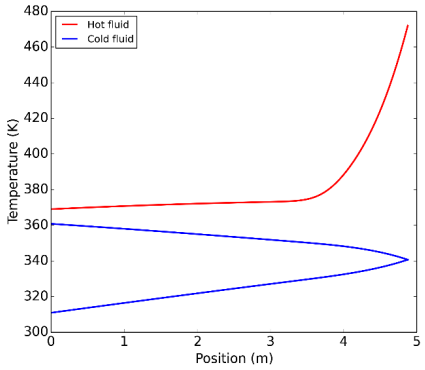

Figure 9: Temperature distribution in 15 s.

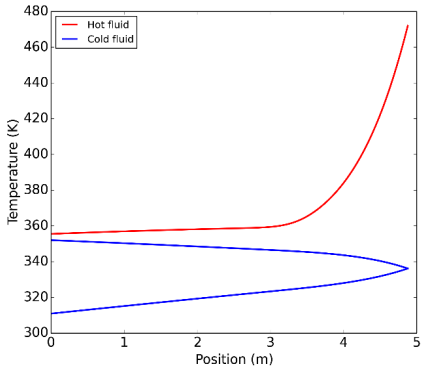

Figure 10: Temperature distribution in 20 s.

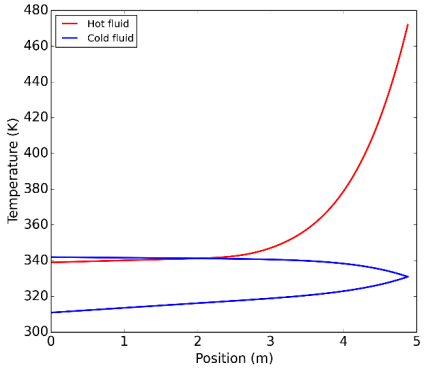

Figure 11: Temperature distribution in 30 s.

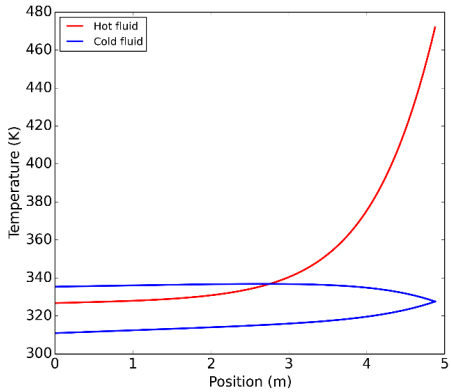

Figure 12: Temperature distribution in 50 s.

The equipment specifications and operating conditions for case 1 are presented in Tables **2** and **3**, respectively.

The difference between case 1 and case 2 lies in the use of SiO_2 nanofluid in the tubes with φ = 3% and dp = 85 nm. Figures **13** and **14** illustrate the temperature profiles for cases 1 and 2 under steady state conditions, respectively. Figures **15** and **16** show the transient temperature profiles of cases 1 and 2, respectively. Figures **17** and **18** demonstrate the film coefficient profiles of case 1 and 2, respectively.

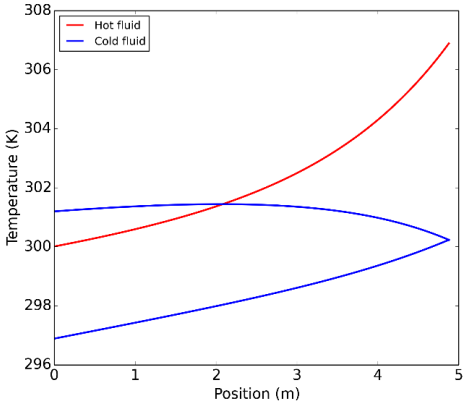

Figure 13: Steady-state Profile Case 1.

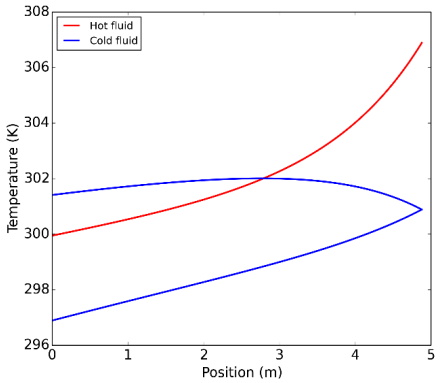

Figure 14: Steady-state Profile Case 2.

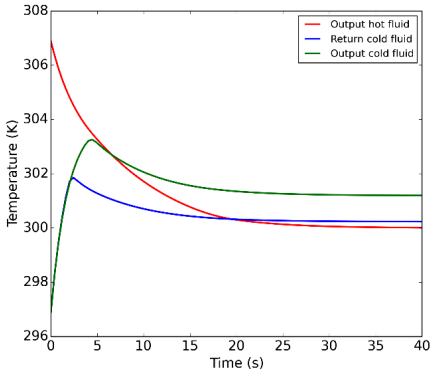

Figure 15: Transient Profile Case 1.

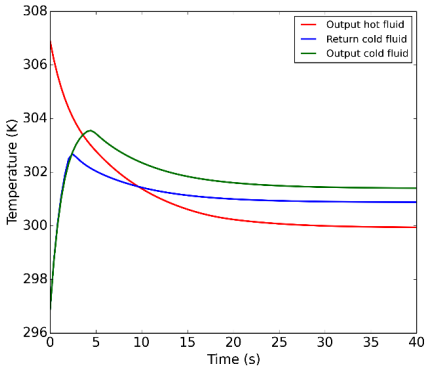

Figure 16: Transient Profile Case 2.

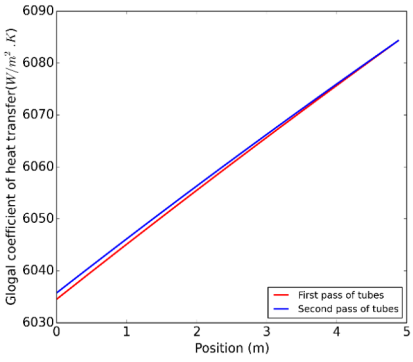

Figure 17: Film Coefficients Case 1.

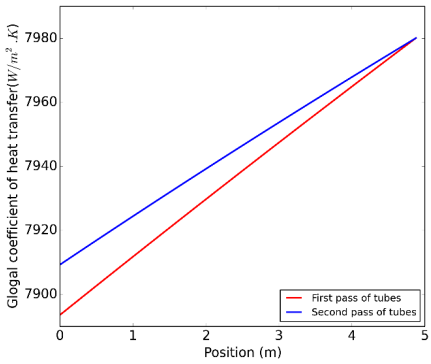

Figure 18: Film Coefficients Case 2.

Table **4** show pressure drop, heat flow and Ft of the simulations.

Table 4: Pressure Drop, Heat Flow and Ft

	Case 1	Case 2
Shell	55.263 kPa	55.263 kPa
Tube	55.707 kPa	53.954 kPa
Q	720.783 kW	726.805 kW
Ft	0.593	0.471

5. DISCUSSION

The simulated cases provided relevant data for analysis and designing purposes. They are tools that assist in defining the optimum operating conditions, considering the offered heat flow, the pressure losses and the inversion region.

Even though the presence of suspended particles had significant influence on both the thermal conductivity and fluid dynamic viscosity, these properties seemed to be independent on their concentration. However, the values obtained for the density and the specific heat were close to those found for hot water, but they presented a small variation as the particles concentration varied.

Figures **13** and **14** show that the inversion region in case 2 is larger than in case 1, which can be confirmed by the Ft value in Table **4**. As recommend by Kern [1], the design of exchangers with multiple passes require high Ft values (Ft ≥ 0.75) in order to prevent temperature inversion regions. In this region, the device does not operate as it should, since the energy flows from the “cold fluid” in the second pass to the “hot fluid”, leading to a reduction in the equipment efficiency. By simulating several different cases, it is

possible to reduce or even eliminate this thermal inversion region. Although it showed a larger inversion region (i.e. lower Ft value), the heat flow obtained in case 2 was close to the one obtained in case 1.

Film coefficient presented values about 30.57 % higher for the SiO_2 nanofluid, whereas no significant differences were noticed in the pressure loss values. In the transient profiles, the tube-pass return temperature was approximately the same as the outflow temperature of the hot fluid in case 1; whereas these temperatures were considerably different in case 2.

Differential transient models and graphics displayed significant temperature peaks inside the equipment. These peaks indicate the existence of great mechanical tension in the metal. So, an interesting criterion for choosing the exchanger material is that it must withstand the stresses caused by the temperature peaks with acceptable deformation. Therefore, as it is of utmost importance in designing the studied heat exchanger, the evaluation of these peaks is one of the important achievements in this work.

Another important variable that must be taken into account is the operational cycle of the exchanger (i.e, how long can it operates between two consecutive maintenances) since the use of nanofluids leads to an increase in fouling, reducing the time between two consecutive maintenances.

Therefore, comparing the two different simulated cases, it can be said that both have similar fluid dynamics and thermal efficiency. Thus, the use of SiO_2 nanofluid is not suitable unless it is part of the production process, as almost no advantage was presented by these simulations over the use of water. In fact, running the exchanger with nanofluids would rather affect its operational cycle by decreasing the time between consecutive maintenances, since fouling is more likely to happen.

CONCLUSIONS

In this work, a transient differential model has been developed for shell-and-tubes heat exchanger with helical baffles 1-2. The model considers one-dimensional variations along the device length. Film coefficients and pressure losses were estimated by using analytical methods found in the literature. The physical properties of the fluids were evaluated locally using prediction equations.

Python framework and its scientific modules were used to assist in the model implementation and simulations. To demonstrate the applicability of the model two operating conditions were simulated using the same equipment. The use of computational models saves resources, since we can perform various simulations in order to determine the best operating conditions of this equipment in a shorter time and avoiding real tests.

The simulations used water / water and SiO_2 / water nanofluid to analyze both the thermal and fluid dynamics behavior of the equipment. The integral analytical methods employ average or “caloric” temperatures for estimating the physical properties of the fluids. This particular technique is quite accurate when dealing with water, but it might generate large deviations for viscous fluids. Thus, the calculation of local properties during the differential model solution makes the equipment sizing / analysis more accurate and reliable.

NOMENCLATURE

Bd	Pitch of helical baffles [*m*]
C	Specific Heat of fluid in shell [*J*/*Kg*.*K*]
c	Specific Heat of fluid in tubes [*J*/*Kg*.*K*]
Db	Diameter of nozzles [*m*]
de	Outer diameter of tubes [*m*]
di	Inner diameter of tubes [*m*]
DI	Inner diameter of shell [*m*]
df	Diameter of bundle of tubes [*m*]
F_t	Correction factor of LMTD
k	Thermal Conductivity [*W*/*m*.*K*]
LTC	Length of equipment [*m*]
LTO	Length between center of nozzles [*m*]
N_t	Number of tubes
P	Outside perimeter of tube [*m*]
pt	Pitch of tubes [*mm*]
Q	Heat Flow [*KW*]

Re	Reynolds number
Sp	Thickness of baffles [*mm*]
S_c	Cross-section area of shell [m^2]
S_t	Cross-section area of tubes [m^2]
T	Cross-section local in shell [*K*]
T_1_e	Temperature of input of fluid in shell [*K*]
t_1_e	Temperature of input of fluid in tubes [*K*]
t_1	Local temperature in first pass of tubes [*K*]
t_2	Local temperature in second pass of tubes [*K*]
U_1	Convection coefficient local in first pass of tubes [$W/m^2.K$]
U_2	Convection coefficient local in second pass of tubes [$W/m^2.K$]
W	Mass flow of fluid in shell [*Kg*/*s*]
w	Mass flow of fluid in tubes [*Kg*/*s*]

GREEK LETTERS

β	Inclination of helical baflles [*Degrees*]
ρ	Density of fluid [Kg/m^3]
μ	Fluid viscosity at the flow temperature [*Pa.s*]

SUBSCRIPT

t	tube
c	shell
nf	nanofluid
f	fluid

REFERENCES

[1] Kern DQ. Process Heat Transfer, New York: McGraw-Hill 1950.

[2] Tao WQ, He YL and Zhang JF. A Design and Rating Method for Shell-and-Tube Heat Exchangers With Helical Baffles. Journal of Heat Transfer 2010; 132: 51802.1-51802.8.

[3] Schlünder EU. Heat Exchanger Design Handbook. Washington: Hemisphere 1983.

[4] Stehlik P, Nemcansky J and Kral D. Comparison of Correction Factors for Shell-and-Tube Heat Exchangers With Segmental or Helical Baffles. Heat Transfer Eng 1994; 5: 55-65. https://doi.org/10.1080/01457639408939818

[5] Sieder FN and Tate GE. Heat Transfer and Pressure Drop of Liquids in Tubes. Ind Eng Chem 1936; 28: 1429-1433. https://doi.org/10.1021/ie50324a027

[6] Gnielinski V. New Equations for Heat and Mass Transfer in Turbulent Pipe and Channel Flows. Int Chem Eng 1976; 16: 359-368.

[7] Gaddis ES and Gnielinski V. Pressure Drop on the Shell Side of Shell-and-Tube Heat Exchangers with Segmental Baffles. Chem Eng Process 1997; 36: 149-159. https://doi.org/10.1016/S0255-2701(96)04194-3

[8] Kuppan T. Heat Exchanger Design Handbook. New York: Marcel Dekker 2000.

[9] Xiao X, Zhang L, Li X, Jiang B, Yang X and Xia Y. Numerical investigation of helical baffles heat exchanger with different Prandtl number fluids. International Journal of Heat and Mass Transfer 2013; 63: 434-444. https://doi.org/10.1016/j.ijheatmasstransfer.2013.04.001

[10] Perry RH and Green DW. Perry's Chemical Engineers´ handbook. New York: McGraw-Hill, 1999.

[11] Poling BE, Prausnitz JM and O'Connell JP. The properties of gases and liquids. New York: McGraw-Hill 2001.

[12] Xuan Y and Roetzel W. Conceptions for heat transfer correlation of nanofluids. Int J Heat Mass Trans 2000; 43: 3701-3707. https://doi.org/10.1016/S0017-9310(99)00369-5

[13] Sharma KV, Sarma PK, Azmi WH, Mamat R and Kadirgama K. Correlations to predict friction and forced convection heat transfer coefficients of water based nanofluids for turbulent flow in a tube, Int. J. Microscale Nanoscale Therm. Fluid Transport Phenom. (Special Issue in Heat and Mass Transfer in Nanofluids) 2012; 3(4): 1-25.

[14] Vajjha RS, Das DK and Kulkarni DP. Development of new correlations for convective heat transfer and friction factor in turbulent regime for nanofluids. Int J Heat Mass Transf 2010; 53(21-22): 4607-4618. https://doi.org/10.1016/j.ijheatmasstransfer.2010.06.032

[15] Azmi WH, Sharma KV, Sarma PK, Mamat R, Anuar S and Dharma Rao. Experimental determination of turbulent forced convection heat transfer and friction factor with SiO2 nanofluid. Exp Therm Fluid Sci 2013; 51(0): 103e-111. https://doi.org/10.1016/j.expthermflusci.2013.07.006

Received on 12-11-2017 Accepted on 31-01-2018 Published on 25-09-2018

DOI: http://dx.doi.org/10.15377/2409-5826.2018.05.2